Hydrogen bonding and Raman, IR, and 2D-IR spectroscopy of dilute HOD in liquid D_2O

B. Auer, R. Kumar, J. R. Schmidt, and J. L. Skinner†

Theoretical Chemistry Institute and Department of Chemistry, University of Wisconsin, Madison, WI 53706

Edited by Robin M. Hochstrasser, University of Pennsylvania, Philadelphia, PA, and approved May 7, 2007 (received for review February 16, 2007)

We present improvements on our previous approaches for calculating vibrational spectroscopy observables for the OH stretch region of dilute HOD in liquid D_2O. These revised approaches are implemented to calculate IR and isotropic Raman spectra, using the SPC/E simulation model, and the results are in good agreement with experiment. We also calculate observables associated with three-pulse IR echoes: the peak shift and 2D-IR spectrum. The agreement with experiment for the former is improved over our previous calculations, but discrepancies between theory and experiment still exist. Using our proposed definition for hydrogen bonding in liquid water, we decompose the distribution of frequencies in the OH stretch region in terms of subensembles of HOD molecules with different local hydrogen-bonding environments. Such a decomposition allows us to make the connection with experiments and calculations on water clusters and more generally to understand the extent of the relationship between transition frequency and local structure in the liquid.

vibrational spectroscopy | water

Water is ubiquitous in science and nature (1), so it is natural that a tremendous amount of effort has been expended trying to describe and understand the structure and dynamics of its liquid state. Vibrational spectroscopy, both IR and Raman, provides an excellent probe of the local structure in water, because a local mode's vibrational frequency is exquisitely sensitive to the local mode's molecular environment. Actually, the cleanest information about local structure in water comes from the vibrational spectroscopy not of neat water, but rather of dilute HOD in either H_2O or D_2O, because in these cases, respectively, the OD or OH local-mode stretch is almost completely decoupled from the other stretches in the liquid, thus functioning well as a local chromophore. IR and Raman spectra on these systems have been measured by many (2–9).

Valuable information about local dynamics in liquid water can also be obtained from vibrational spectroscopy experiments, in this case of the subpicosecond time-domain variety. On this time scale a local mode's vibrational frequency is continually changing because of molecular dynamics. The resulting dynamic frequency fluctuations, also known as spectral diffusion, can be measured by transient vibrational hole-burning and three-pulse echoes (5, 6, 10–22). In particular, these experiments provide information about both the short-time (stretching) and long-time (making and breaking) aspects of intermolecular hydrogen bonds (23–35).

We and others have developed methods for the theoretical calculation of steady-state and ultrafast vibrational spectroscopy observables (7, 23–27, 36–40). In our approach, the single vibrational mode of interest, for example, the OH stretch of HOD (when it is immersed in D_2O), is treated quantum mechanically, whereas all other degrees of freedom (the bath) are treated classically. Thus we are making the adiabatic approximation in that for a given bath configuration one calculates the instantaneous eigenvalues of the OH stretch, leading to the relevant transition frequencies. The bath degrees of freedom evolve according to Newton's equations during a molecular dynamics simulation, generating a frequency trajectory from which one can calculate spectroscopic observables. To the extent that the transition dipole depends on the bath coordinates [non-Condon effects, which we think are important for water (33)] one also needs to obtain a transition dipole trajectory. The key, then, is to develop methods for calculating the transition frequency and dipole accurately and quickly for each bath configuration. For water we have suggested that both the frequency and dipole are approximately linearly related to the electric field from the surrounding waters, and the coefficients have been determined from quantum chemical calculations on clusters (25, 33, 35, 36). This approach has provided reasonable (although by no means perfect) agreement with experiment.

One of the purposes of this article is to report improvements on our previous methods. The improvements are 4-fold: (*i*) our electronic structure benchmarks involve larger and more clusters; (*ii*) the electrostatic (point charge) effects of the water molecules surrounding each cluster are now included in the electronic structure calculations, ameliorating extrapolation issues; (*iii*) for each cluster anharmonic transition frequencies are calculated more accurately (using a discrete variable representation approach instead of fitting to a Morse potential); and (*iv*) a more accurate (quadratic instead of linear) fit of the benchmark frequencies to the electric field is proposed. With these improvements we recalculate experimental observables (Raman and IR spectra, three-pulse echo peak shift, and 2D-IR spectra) for HOD in D_2O by using the SPC/E water simulation model (41), finding in all cases modest improvements [over our previous calculations (35)] in the agreement with experiment.

The second purpose of this article is to understand better how the OH transition frequency is related to the H-bond configuration of the HOD molecule in the liquid. For years one has generally understood that molecules with weak or broken H-bonds (to the H of HOD) absorb on the blue side of the spectrum, whereas molecules with strong H-bonds absorb on the red. Renewed interest in a more detailed understanding of this general trend is motivated by the recent x-ray Raman, absorption, and emission experiments (42–49), some interpretations of which (46, 49) suggest a picture of H-bonding in liquid water quite different from the traditional one of more or less tetrahedral coordination with ≈3.5 H-bonds per molecule. The proposed picture is one of rings and chains of connected water molecules, each of which makes one strong donating and one strong accepting H-bond (46, 49). A crucial aspect of evaluating this scenario comes from assessing whether this picture is compatible with vibrational spectroscopy (50, 51). A second motivating factor for a better understanding of the relationship between transition frequency and local structure in the liquid comes from beautiful experiments and calculations on water clusters (52–59) showing clearly that vibrational frequencies of

Author contributions: J.L.S. designed research; and B.A., R.K., and J.R.S. performed research.

The authors declare no conflict of interest.

This article is a PNAS Direct Submission.

†To whom correspondence should be addressed. E-mail: skinner@chem.wisc.edu.

© 2007 by The National Academy of Sciences of the USA

the OH stretch depend on much more than the geometry of the donor–acceptor pair; rather, they also depend on the number and nature of other H-bonds to the donor and acceptor molecules and indeed to the H-bonding configuration extending at least several solvation shells from the donor–acceptor pair. These complicated dependences arise from the cooperative nature of H-bonding interactions.

To shed some light on this issue, we decompose the distribution of OH stretch frequencies for the full ensemble of HOD molecules into subdistributions for HOD molecules with different H-bonding environments. Such a decomposition does not imply support for a mixture model of water; it simply is a way to classify instantaneous configurations. For such a decomposition one needs an H-bond definition, for which there are many proposals in the literature (46, 60–63). We have recently proposed an H-bonding definition (64) based on the electronic structure of water dimers (65), which involves the O—H distance of the donor–acceptor pair, and the orientation of the acceptor molecule (in electronic structure parlance often called the electron donor). Thus we decompose the distribution of frequencies into subdistributions with different H-bonding configurations based on this definition, which has some relevance with regard to the compatibility of the IR and Raman spectra with recent x-ray absorption experiments and to the cluster results and their extrapolation to the liquid (57, 59).

OH Stretch Transition Frequency, Dipole, and Polarizability

In our approach to the vibrational spectroscopy of dilute chromophores in liquids, the first step is to generate clusters, in this case HOD molecules surrounded by D_2O molecules. To this end, we run a molecular dynamics simulation of 128 SPC/E D_2O molecules in the NVE ensemble, equilibrated to 300 K, as described (25, 33, 35, 36). Note that the experimental molecular number density at 1 atm pressure (1 atm = 101.3 kPa) is essentially the same for both water and heavy water; herein we use the value for heavy water of $3.32 \times 10^{28}/m^3$. For OH stretch frequency calculations we will imagine that one of the D atoms is an H. Thus we randomly tag a D atom on one of the molecules, and to generate clusters we retain all other water molecules whose O atoms are within 4 Å of the H (tagged D). Full electronic structure calculations will be performed on the molecules in the cluster. In addition, we record the positions of the nuclei of all other water molecules within half the box length; these nuclei will be point charges (keeping their SPC/E values) in the electronic structure calculations. Note, then, that this procedure for selecting clusters differs slightly from our previous one (one difference is that the average cluster size, now 9.25, is larger), and that in the past we did not include the point charges in the electronic structure calculations.

We then perform electronic structure calculations (B3LYP/6–311++G**) on 999 such randomly selected clusters, in the presence of the surrounding point charges. For these calculations all nuclei are fixed at their positions in the simulation, except that the OH stretch coordinate is varied (keeping the center of mass of the HOD molecule fixed). This maps out the 1D Born–Oppenheimer potential for the OH stretch, whose eigenvalues are solved by using the discrete variable representation and a pseudodiatomic H—OD reduced mass of 0.954426 atomic mass units. Note that implementing this procedure for the isolated HOD molecule (OD distance and bond angle are kept at their SPC/E values), yields an OH stretch fundamental frequency of ω_{10} = 3,717 cm^{-1}, in good agreement with the experimental value of 3,707 cm^{-1}. In what follows, all calculated frequencies are then scaled by 0.9973 (obtained from the ratio of these two numbers) to correct for this small error.

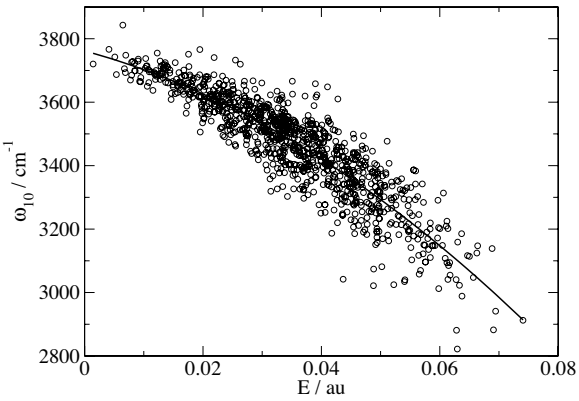

Fig. 1. Calculated OH stretch frequencies, ω_{10}, for HOD/D_2O clusters and point charges of surrounding water molecules, versus electric *E*. Solid line is the best quadratic fit.

As in the past, we now correlate these frequencies with the component of the electric field parallel to the OH bond, evaluated at the H atom, from the (SPC/E) point charges of all molecules in the configuration (except the HOD molecule) within half the box length. In the past we used a linear correlation. Here, however, we find that a quadratic dependence produces a slightly better fit. The results of this fit, compared with the *ab initio* results, are shown in Fig. 1, and the formula for the fit is given in Table 1. Although the fit is reasonable there still exists considerable scatter (rmsd is 70.1 cm^{-1}). Note that this rmsd is slightly larger than our earlier value (35), but now, because all molecules within half the box length are included in calculating the electric field, we have no residual extrapolation error as we did previously. We then rerun a simulation, randomly choosing D atoms as surrogate H atoms, calculate the electric field from all molecules within half the box length, and use the formula to relate field to frequency. This process generates a distribution of frequencies from the liquid, which is compared with the actual distribution of *ab initio* frequencies from the embedded cluster calculations (Fig. 2). The comparison is really very good, showing that even though there is quite of bit of

Table 1. Empirical relationships for the transition frequencies, dipole and polarizability derivatives (normalized by their gas-phase values), and matrix elements

Empirical relationship	*R*	rms error
ω_{10} = 3,761.6 cm^{-1} − 5,060.4 cm^{-1}/a.u. E − 86,225 cm^{-1}/a.u.^{2} E^2	0.90	70.1 cm^{-1}
ω_{21} = 3,614.1 cm^{-1} − 5,493.7 cm^{-1}/a.u. E − 115,670 cm^{-1}/a.u.^{2} E^2	0.90	84.7 cm^{-1}
x_{10} = 0.1024 Å − 0.927 × 10^{-5} Å/cm^{-1} ω_{10}	1.00	5.9 × 10^{-5} Å
x_{21} = 0.1428 Å − 1.29 × 10^{-5} Å/cm^{-1} ω_{21}	1.00	1.43 × 10^{-4} Å
μ'/μ_g' = 0.71116 + 75.591 a.u.$^{-1}$ E	0.92	0.41
α'/α_g' = 1.2142 + 3.6206 a.u.$^{-1}$ E	0.31	0.14

The electric field, *E*, at the H and in the direction of the OH bond, is in a.u.: frequencies are in cm^{-1}; and the matrix elements, x_{10} and x_{21}, are in Å. The correlation coefficient, *R*, and rms error of each fit are also listed.

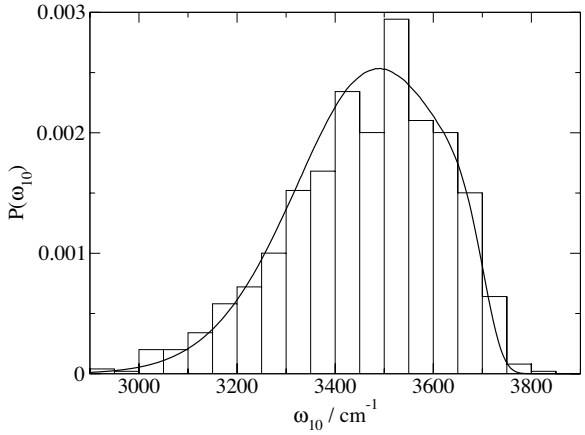

Fig. 2. Distribution of calculated OH stretch frequencies from 999 clusters and point charges of surrounding water molecules (histogram) and from the electric field fit (solid line).

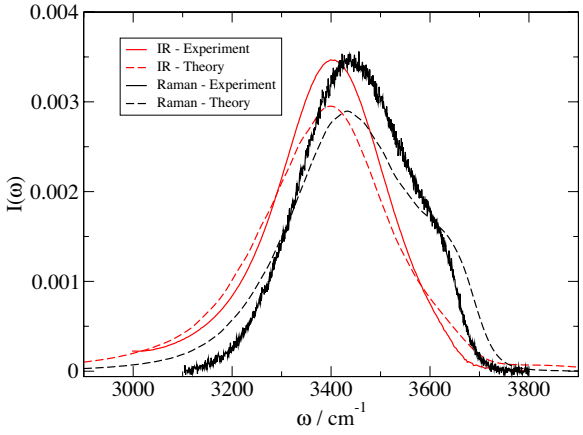

Fig. 3. Experimental (5, 7) and calculated Raman and IR line shapes for HOD in liquid D_2O at 300 K.

inaccuracy from using the field to predict the frequency for individual configurations, on the average the formula produces a reasonably accurate distribution of frequencies. We also perform a similar quadratic fit for ω_{21}, which is needed for the nonlinear spectroscopy calculations (Table 1).

As in the past we write the projection of the transition dipole for vibrational states i and j in the direction of the external (light) electric field as:

$$\mu_{ij} = \mu' x_{ij} \hat{u} \cdot \hat{\epsilon}, \qquad [1]$$

where μ' is the dipole derivative, x is the OH stretch coordinate, $\hat{u}$ is the OH bond vector, and $\hat{\epsilon}$ is the direction of the external electric field. For the clusters μ' is obtained from the electronic structure calculations, and the matrix elements x_{ij} are obtained from the discrete variable representation analysis. As before, μ' and x_{ij} are then fit to the electric field and frequency ω_{ij}, respectively, with results shown in Table 1. These results are slightly different from those reported earlier, because of our somewhat different procedures for obtaining the frequencies. For the isotropic Raman spectrum we also need the polarizability; as before the polarizability derivative is obtained from electronic structure calculations and then correlated with the electric field as shown in Table 1.

IR, Raman, and 2D-IR Spectra and Echo Peak Shift

Spectroscopic observables are calculated from frequency and transition dipole (polarizability) trajectories as in previous work (35). As such, non-Condon and motional narrowing effects are included. As before, the OH stretch fundamental lifetime is taken to be 700 fs (5). Experimental IR and Raman line shapes (5, 7), slightly corrected from the experimental cross-sections and scattering intensities as described (35), are shown in Fig. 3, together with our theoretical calculations. Note that although the experimental Raman line shape is from the unpolarized signal (7) (whereas the theoretical result is for the isotropic line shape), in this particular instance the difference between these two is quite small (8, 9). The agreement between theory and experiment for the peak positions in both Raman and IR is excellent, hence the experimental red shift in going from Raman to IR is also properly described. The experimental difference in line shape between IR and Raman is also reproduced by the theory, although the theoretical shoulder in the Raman line shape is slightly too accentuated. The biggest discrepancy between theory and experiment is in the line widths, which are on the order of 10% too large in the theory. The comparison between theory and experiment shown herein represents a modest improvement over our previous results (35). A full discussion of the features of, and differences between, the IR and Raman line shapes has been given in ref. 35. Here, one might simply note that the substantial differences between the theoretical line shapes and the frequency distribution (see Fig. 2) arise from non-Condon and motional narrowing effects.

Theoretical [calculated as described (35)] and experimental results for the three-pulse echo peak shift (5) are shown in Fig. 4. One sees quantitative agreement with experiment at short (<50 fs) times and qualitative agreement thereafter. In particular, the theoretical recurrence occurs at 100 fs, whereas the experimental recurrence is at 150 fs (5), and the longtime decay of the theoretical peak shift is slightly too fast in comparison with experiment. Discrepancies between theory and experiment are caused by inadequacies of the SPC/E model and/or inaccuracies of our spectroscopic calculations. We are more inclined to believe the former, but certainly cannot rule out the latter. In any case, these theoretical peak shift results are again a modest improvement (in comparison with experiment) over our previous calculations for the same water model (35). Full 2D-IR calculations for this model are shown in Fig. 5, which are qualitatively the same as those shown previously (35) and qualitatively the same as from experiment (20, 21). These 2D-IR spectra can be analyzed in a number of different ways (66),

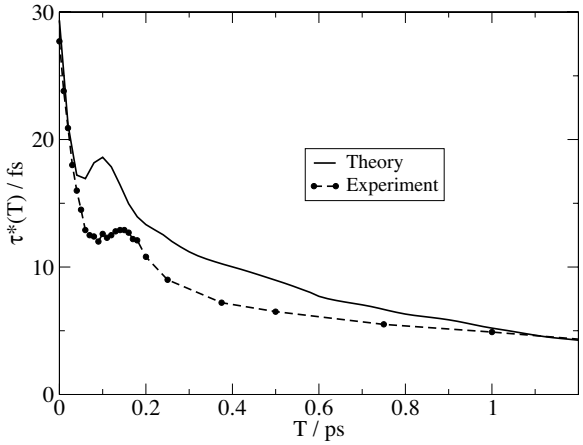

Fig. 4. Experimental (21) and calculated three-pulse vibrational echo peak shift for HOD in liquid D_2O at 300 K.

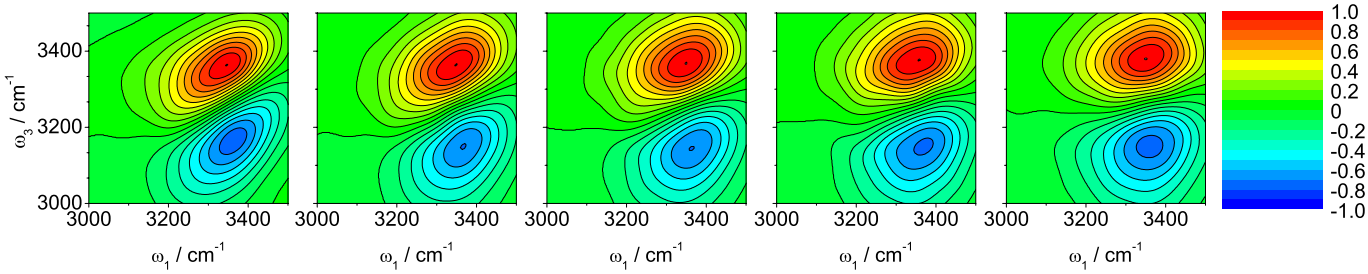

Fig. 5. Calculated 2D-IR spectra as described in the text for HOD in liquid D_2O at 300 K. The five images correspond, from left to right, to the waiting times of $T = 0$, 100, 200, 400, and 800 fs.

including by considering the nodal slope between the 0-1 and 1-2 resonances (21, 35).

OH Stretch Frequency and Hydrogen-Bonding Configuration

According to our theoretical calculations, the overall distribution of OH stretch frequencies in the liquid is given by the solid line in Fig. 2. As mentioned in the Introduction, we can decompose this distribution into subdistributions based on the H-bonding configurations of the HOD molecule. The classification of the configurations can be quite complex, involving several solvation shells of the HOD molecule. For this study, however, we will focus on the H-bonding state only of the HOD molecule itself. To this end, we can describe the H-bonding configuration of the HOD molecule by the number of H-bonds from neighboring molecules to the O atom, n_O, the number of H-bonds to the H atom, n_H, and the number of H-bonds to the D atom, n_D. Note that for configurations generated from an SPC/E simulation and reasonable H-bond definitions $n_O = 0$, 1, 2, 3 and n_H or $n_D = 0$, 1, 2. Thus every HOD molecule can be assigned to one of 36 classes.

This large number of classes makes it difficult to visualize and discuss results. However, because the probability of obtaining either $n_O = 0$ or 3 is small, we can profitably define a new number N_O, which is 1 if n_O is 0 or 1, and 2 if n_O is 2 or 3. Thus molecules with $N_O = 1$ correspond for the most part to those with one H-bond to the O, whereas molecules with $N_O = 2$ correspond for the most part to those with two H-bonds to the O. Likewise, the probability of obtaining $n_H = 2$ is small, and so we can define a new number N_H, which is 0 if $n_H = 0$, and 1 if $n_H = 1$ or 2, and similarly for D. This then gives a more manageable number of eight H-bond classes, each of which is described by the triplet of numbers N_O, N_H, and N_D.

Alternatively, we can describe each class by the total number of H-bonds $N_O + N_H + N_D$, the number of H-bond donors $N_H + N_D$, and if there is a single donor (in which case the latter number is 1), whether it is the H or the D. Thus, for example, the triplet $N_O = 2$, $N_H = 1$, and $N_D = 0$ can be labeled 3_{SH} (three H-bonds with the single donor being the H). (Note, however, that because of the way we have combined the original 36 classes, a member of the class 3_{SH} will occasionally have four H-bonds.) The translation between these two different ways of labeling environments is given in Table 2, where D (as the first letter) means double donor, S means single donor, and N means nondonor.

Table 2. Statistics of the frequency subdistributions

N_O	N_H	N_D	Label	$\langle\omega_{10}\rangle$	f
1	0	0	1_N	3,654	0.014
1	0	1	2_{SD}	3,665	0.056
1	1	0	2_{SH}	3,458	0.056
1	1	1	3_D	3,473	0.227
2	0	0	2_N	3,610	0.013
2	0	1	3_{SD}	3,624	0.080
2	1	0	3_{SH}	3,381	0.080
2	1	1	4_D	3,400	0.475

N_O, N_H, and N_D are described in the text. Each subdistribution is labeled as described in the text. $\langle\omega_{10}\rangle$ is the average frequency (in cm^{-1}) of each subdistribution, and f is the fraction of molecules in each subdistribution.

To perform this classification for an HOD molecule in the liquid, we need to be able to specify how many H-bonds each of its atoms is involved with. For this we turn to our proposed H-bond definition (64) based on the electronic occupancy of OH antibonding orbitals (67). For a water monomer the occupancies of its two OH antibonding orbitals are essentially zero. For an H atom (donor) involved in an H-bond, however, the occupancy of its OH antibonding orbital can be appreciable, because of electron donation from the lone pairs of the acceptor molecule (67). For a given pair of H and O atoms on different molecules we have shown, using electronic structure calculations, that this occupancy depends primarily on two variables related to the relative geometry of these two molecules (64). One variable is r, the H—O intermolecular distance. The second is the angle that the intermolecular OH ray makes with the out-of plane unit vector (in the direction of the p_z orbital) on the acceptor molecule (64). ψ is defined to be the smaller of this angle and its complement. The map is given by (64):

$$N(r, \psi) = \exp(-r/0.343\ \text{Å})\ (7.1 - 0.050\ \psi + 0.00021\ \psi^2), \quad [2]$$

where N is the occupancy and ψ is in degrees. We have calculated (64) the distribution of occupancies for all intermolecular O—H pairs in the liquid, and from its bimodal structure we have suggested a critical occupancy of 0.0085. Therefore, for every (intermolecular) pair of H and O atoms in the H_2O liquid, one defines the coordinates r and ψ and calculates the occupancy N according to the above; if $N > 0.0085$, these atoms are H-bonded (and if $N < 0.0085$, they are not). According to this definition, for liquid H_2O at 300 K and 1 atm pressure $\langle n_H\rangle = 0.84$, and $\langle n_O\rangle = 2\langle n_H\rangle = 1.68$, so that the average number of H-bonds associated with a given molecule is $\langle n_O\rangle + 2\langle n_H\rangle = 3.36$ (64). Furthermore, the fractions of molecules with one, two, three, four, or five H-bonds are 0.017, 0.126, 0.372, 0.449, and 0.036, respectively.

Finally, then, for the purpose of the frequency calculations for HOD in D_2O, we randomly tag D atoms in the D_2O simulation to be surrogate H atoms. For a given configuration of the HOD molecule in the liquid, N_O, N_H, and N_D are determined as described above. At the same time the OH stretch frequency is calculated as described above. This process is repeated many times, leading to a distribution of OH stretch frequencies for each H-bonded class. The eight subdistributions are shown in Fig. 6, together with the overall frequency distribution. The subdistributions are not normalized individually; thus subdistributions sum to give the overall distribution. Each subdistribution

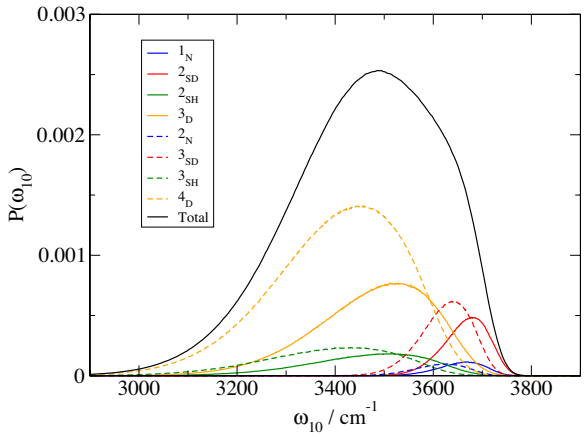

Fig. 6. Distributions of OH stretch frequencies, as calculated from the electric field fit, for eight different classes of H-bonded HOD molecules.

can be characterized by its average frequency, and the fraction of molecules it contains, as shown in Table 2.

From Fig. 6 or Table 2 one can see what happens to the OH stretch frequency when a hydrogen bond to the H is added (N_H goes from 0 to 1, keeping N_O and N_D unchanged): the average OH stretch frequency is red-shifted by anywhere from 192 to 229 cm^{-1}. Similarly, when an H-bond to the O is added (N_O goes from 1 to 2), the average frequency is red-shifted by anywhere from 41 to 77 cm^{-1}, and when an H-bond to the D is added (N_D goes from 0 to 1), the average frequency is blue-shifted by anywhere from 11 to 19 cm^{-1}. Consequently it follows that the 2_{SD} distribution is the least red-shifted (from the gas-phase frequency of 3,707 cm^{-1}), and 3_{SH} is the most red-shifted. The frequency ordering of all of the distributions can be read off of Table 2. Interestingly, this ordering shares some features with that from the recent paper by Lenz and Ojamäe (57) obtained with an extrapolation from calculations on H_2O clusters. In particular, the frequency ordering $3_{SH} < 4_D < 3_D$ is found in both cases. The same conclusion is also found in the interesting theoretical and experimental paper on water clusters by Ohno *et al.* (59). In light of the results in both of these cluster papers it seems likely that the large breadth of each of our four H-bonded (to the H) subensembles can be attributed in part to different H-bonding configurations of the acceptor molecule.

It is important to reiterate that for each HOD molecule the frequency calculation is obtained from the electric field fit, which has significant scatter compared with the benchmark frequencies, as discussed above. Thus it would be better if we could use the benchmark frequencies themselves (rather than those from the electric field map) to investigate these distributions. Evidently, however (see Fig. 2), 999 clusters are not enough to obtain even a good overall distribution of frequencies, much less good subdistributions. To obtain reasonable subdistributions from benchmarks would take tens of thousands of clusters. Also note that, in general, line shapes are not simply frequency distributions, because of the complications of non-Condon effects and motional narrowing. Despite these realities, we believe that one can draw two further conclusions from the above. First, from summing the relative probabilities of the different classes, we find that the fraction of double donors is 0.702, the fraction of single donors is 0.272, and the fraction of nondonors is 0.027. If the fraction of single donors were substantially higher, as claimed by Wernet *et al.* (46), and of course making the big assumption that the shapes and positions of these subdistributions are invariant to the particular microscopic model of water, the amplitudes of the four single donor distributions would be increased at the expense of the two double donor distributions, leading to a dramatic change in the shape of the overall distribution. In particular, the 2_{SD} and 3_{SD} distributions peak at the relatively high values of 3,665 and 3,624 cm^{-1}, respectively, because these correspond to "dangling" OH groups. A large fraction of single donors would then imply strong spectral intensity ≈3,650 cm^{-1}, and maybe even a doubly peaked spectrum (51), which is not seen experimentally. Second, the eight subdistributions are broad and overlapping, implying that the structural origins of the line shapes are complicated. A corollary, of course, is that detailed structural inferences from line shape features must be drawn with care.

Summary

Advances in our theoretical approach for describing liquid-state spectroscopy have led to improved results (in comparison with experiment) for 1D and 2D line shapes for dilute HOD in liquid D_2O. The theoretical distribution of frequencies has been decomposed into subensembles for different H-bonding environments of the HOD molecules, each of which peak at a different frequency. The still quite substantial breadth of four of these subdistributions is presumably caused in part by different H-bonding configurations of the acceptor and other D_2O molecules. Our theoretical results indicate that the fraction of HOD molecules that are single donors is ≈27%, and we suggest that if, in fact, this fraction was significantly higher, the resulting vibrational line shapes would not be compatible with experiment.

We thank Prof. Will Polik and Hope College (Holland, MI) for the use of their MU3C computer cluster on which some of the calculations reported herein were performed and Prof. Lars G. M. Pettersson and Mathias Ljungberg for helpful discussion. This work was supported by National Science Foundation Grant CHE-0446666, an American Chemical Society/Petroleum Research Fund AC grant, and a Hertz fellowship (to J.R.S.).

1. Ball P (1999) *Life's Matrix: A Biography of Water* (Farrar, Straus, and Giroux, New York).
2. Falk M, Ford TA (1966) *Can J Chem* 44:1699–1707.
3. Walrafen GE (1968) *J Chem Phys* 48:244–251.
4. Wang Z, Pakoulev A, Pang Y, Dlott DD (2004) *J Phys Chem A* 108:9054–9063.
5. Fecko CJ, Loparo JJ, Roberts ST, Tokmakoff A (2005) *J Chem Phys* 122:054506.
6. Asbury JB, Steinel T, Stromberg C, Corcelli SA, Lawrence CP, Skinner JL, Fayer MD (2004) *J Phys Chem A* 108:1107–1119.
7. Smith JD, Cappa CD, Wilson KR, Cohen RC, Geissler PL, Saykally RJ (2005) *Proc Natl Acad Sci USA* 102:14171–14174.
8. Murphy WF, Bernstein HJ (1972) *J Phys Chem* 76:1147–1152.
9. Scherer JR, Go MK, Kint S (1974) *J Phys Chem* 78:1304–1313.
10. Graener H, Seifert G, Laubereau A (1991) *Phys Rev Lett* 66:2092–2095.
11. Woutersen S, Emmerichs U, Bakker HJ (1997) *Science* 278:658–660.
12. Bakker HJ, Woutersen S, Nienhuys H-K (2000) *Chem Phys* 258:233–245.
13. Laenen R, Rauscher C, Laubereau A (1998) *Phys Rev Lett* 80:2622–2625.
14. Gale GM, Gallot G, Hache F, Lascoux N, Bratos S, Leicknam J-C (1999) *Phys Rev Lett* 82:1068–1071.
15. Nienhuys H-K, Woutersen S, vanSanten RA, Bakker HJ (1999) *J Chem Phys* 111:1494–1500.
16. Bratos S, Gale GM, Gallot G, Hache F, Lascoux N, Leicknam J-C (2000) *Phys Rev E* 61:5211–5217.
17. Stenger J, Madsen D, Hamm P, Nibbering ETJ, Elsaesser T (2002) *J Phys Chem A* 106:2341–2350.
18. Asbury JB, Steinel T, Kwak K, Corcelli SA, Lawrence CP, Skinner JL, Fayer MD (2004) *J Chem Phys* 121:12431–12446.
19. Fecko CJ, Eaves JD, Loparo JJ, Tokmakoff A, Geissler PL (2003) *Science* 301:1698–1702.
20. Loparo JJ, Roberts ST, Tokmakoff A (2006) *J Chem Phys* 125:194521.
21. Eaves JD, Loparo JJ, Fecko CJ, Roberts ST, Tokmakoff A, Geissler PL (2005) *Proc Natl Acad Sci USA* 102:13019–13022.
22. Steinel T, Asbury JB, Corcelli SA, Lawrence CP, Skinner JL, Fayer MD (2004) *Chem Phys Lett* 386:295–300.
23. Lawrence CP, Skinner JL (2003) *Chem Phys Lett* 369:472–477.

24. Lawrence CP, Skinner JL (2003) *J Chem Phys* 118:264–272.
25. Corcelli SA, Lawrence CP, Skinner JL (2004) *J Chem Phys* 120:8107–8117.
26. Rey R, Møller KB, Hynes JT (2002) *J Phys Chem A* 106:11993–11996.
27. Møller KB, Rey R, Hynes JT (2004) *J Phys Chem A* 108:1275–1289.
28. Piryatinski A, Lawrence CP, Skinner JL (2003) *J Chem Phys* 118:9664–9671.
29. Piryatinski A, Lawrence CP, Skinner JL (2003) *J Chem Phys* 118:9672–9679.
30. LaCour Jansen T, Hayashi T, Zhuang W, Mukamel S (2005) *J Chem Phys* 123:114504.
31. Schmidt JR, Corcelli SA, Skinner JL (2004) *J Chem Phys* 121:8887–8896.
32. Corcelli SA, Lawrence CP, Asbury JB, Steinel T, Fayer MD, Skinner JL (2004) *J Chem Phys* 121:8897–8900.
33. Schmidt JR, Corcelli SA, Skinner JL (2005) *J Chem Phys* 123:044513.
34. Eaves JD, Tokmakoff A, Geissler PL (2005) *J Phys Chem A* 109:9424–9436.
35. Schmidt JR, Roberts ST, Loparo JJ, Tokmakoff A, Fayer MD, Skinner JL (2007) *Chem Phys*, in press.
36. Corcelli SA, Skinner JL (2005) *J Phys Chem A* 109:6154–6165.
37. Hermansson K, Knuts S, Lindgren J (1991) *J Chem Phys* 95:7486–7496.
38. Lawrence CP, Skinner JL (2002) *J Chem Phys* 117:8847–8854.
39. Hayashi T, LaCour Jansen T, Zhuang W, Mukamel S (2005) *J Phys Chem A* 109:64–82.
40. Harder E, Eaves JD, Tokmakoff A, Berne BJ (2005) *Proc Natl Acad Sci USA* 102:11611–11616.
41. Berendsen HJC, Grigera JR, Straatsma TP (1987) *J Phys Chem* 91:6269–6271.
42. Wilson KR, Rude BS, Catalano T, Schaller RD, Tobin JG, Co DT, Saykally RJ (2001) *J Phys Chem B* 105:3346–3349.
43. Myneni S, Luo Y, Näslund LÅ, Cavalleri M, Ojamäe L, Ogasawara H, Pelmenschikov A, Wernet P, Väterlein P, Heske C, *et al.* (2002) *J Phys Condens Matter* 14:213–219.
44. Bergmann U, Wernet P, Glatzel P, Cavalleri M, Pettersson LGM, Nilsson A, Cramer SP (2002) *Phys Rev B* 66:092107.
45. Guo J-H, Luo Y, Augustsson A, Rubensson J-E, Säthe C, Ågren H, Siegbahn H, Nordgren J (2002) *Phys Rev Lett* 89:137402.
46. Wernet P, Nordlund D, Bergmann U, Cavalleri M, Odelius M, Ogasawara H, Näslund LÅ, Hirsch TK, Ojamäe L, Glatzel P, *et al.* (2004) *Science* 304:995–999.
47. Smith JD, Cappa CD, Wilson KR, Messer BM, Cohen RC, Saykally RJ (2004) *Science* 306:851–853.
48. Kashtanov S, Augustsson A, Luo Y, Guo J-H, Säthe C, Rubensson J-E, Siegbahn H, Nordgren J, Ågren H (2004) *Phys Rev B* 69:024201.
49. Näslund L-Å, Lüning J, Ufuktepe Y, Ogasawara H, Wernet P, Bergmann U, Pettersson LGM, Nilsson A (2005) *J Phys Chem B* 109:13835–13839.
50. Leetmaa M, Ljungberg M, Ogasawara H, Odelius M, Näslund L-Å, Nilsson A, Pettersson LGM (2006) *J Chem Phys* 125:244510.
51. Smith JD, Cappa CD, Messer BM, Drisdell WS, Cohen RC, Saykally RJ (2006) *J Phys Chem B* 110:20038–20045.
52. Xantheas SS (2000) *Chem Phys* 258:225–231.
53. Buch V, Bauerecker S, Devlin JP, Buck U, Kazimirski JK (2004) *Int Rev Phys Chem* 23:375–433.
54. Fanourgakis GS, Aprà E, deJong WA, Xantheas SS (2005) *J Chem Phys* 122:134304.
55. Dahlke EE, Truhlar DG (2006) *J Phys Chem B* 110:10595–10601.
56. Anick DJ (2006) *J Phys Chem A* 110:5135–5143.
57. Lenz A, Ojamäe L (2006) *J Phys Chem A* 110:13388–13393.
58. Pedulla JM, Vila F, Jordan KD (1996) *J Chem Phys* 105:11091–11099.
59. Ohno K, Okimura M, Akai N, Katsumoto Y (2005) *Phys Chem Chem Phys* 7:3005–3014.
60. Luzar A, Chandler D (1996) *Phys Rev Lett* 76:928–931.
61. Luzar A, Chandler D (1996) *Nature* 379:55–57.
62. Lee H-S, Tuckerman ME (2006) *J Chem Phys* 125:154507.
63. Kuo I-FW, Mundy CJ (2004) *Science* 303:658–660.
64. Kumar R, Schmidt JR, Skinner JL (2007) *J Chem Phys* 126:204107.
65. Reed AE, Weinhold F (1983) *J Chem Phys* 78:4066–4073.
66. Roberts ST, Loparo JJ, Tokmakoff A (2006) *J Chem Phys* 125:084502.
67. Weinhold F, Landis C (2005) *Valency and Bonding: A Natural Bond Orbital Donor-Acceptor Perspective* (Cambridge Univ Press, Cambridge, UK).